Journal of Sound and Vibration 383 (2016) 35–45

Contents lists available at ScienceDirect

Journal of Sound and Vibration

journal homepage: www.elsevier.com/locate/jsvi

Stress tracking in thin bars by eigenstrain actuation

J. Schoeftner*, H. Irschik

Johannes Kepler University Linz, Institute of Technical Mechanics, Altenberger Strasse 69, A-4040 Linz, Austria

ARTICLE INFO

Article history:
Received 22 January 2016
Received in revised form
22 June 2016
Accepted 18 July 2016
Handling Editor: D.J. Wagg
Available online 12 August 2016

Keywords:
Stress tracking
Stress control
Eigenstrain
Eigenstress
Piezoelectricity
Longitudinal vibrations
Linear elastic bar

ABSTRACT

This contribution focuses on stress tracking in slender structures. The axial stress distribution of a linear elastic bar is investigated, in particular, we seek for an answer to the following question: in which manner do we have to distribute eigenstrains, such that the axial stress in a bar is equal to a certain desired stress distribution, despite external forces or support excitations are present? In order to track a certain time- and space-dependent stress function, smart actuators, such as piezoelectric actuators, are needed to realize eigenstrains. Based on the equation of motion and the constitutive relation, which relate stress, strain, displacement and eigenstrains, an analytical solution for the stress tracking problem is derived. The starting point for the derivation of a solution for the stress tracking problem is a semi-positive definite integral depending on the error stress which is the difference between the actual stress and the desired stress. Our derived stress tracking theory is verified by two examples: first, a clamped–free bar which is harmonically excited is investigated. It is shown under which circumstances the axial stress vanishes at every location and at every time instant. The second example is a support-excited bar with end mass, where a desired stress profile is prescribed.

1. Introduction

Engineering mechanics is the discipline that calculates the displacements, strains and stresses, which are caused by a given set of loadings. These imposed loadings can be divided into body forces, surface tractions or imposed boundary excitations. In the dynamic case, initial conditions may be regarded as additional disturbances for the deformations of elastic bodies. These systems are fully described by partial differential equations and proper initial and boundary conditions. Within the framework of a linear theory of elasticity, the reader is referred to Hetnarski and Ignaczak [1], Gurtin [2], Lurie [3] and Ziegler [4].

For the development of control methods, sensing and structural health monitoring, piezoelectric transducers are well-established devices, see e.g. Moheimani and Fleming [5]. Classical review works on this subject are given by Crawley [6], Miu [7] and Tzou [8]. Recently, driven by the technological developments in the field of piezoelectricity, we ask how to design an actuating piezoelectric control device, so that a certain stress field is obtained. In other words, the spatial distribution and the transient actuation of a control piezoelectric device need to be computed, so that a certain desired stress distribution is obtained. If a mathematical model of a given dynamical system is available, an inversely posed problem needs to be solved: one asks for the control actuation in order to track a certain stress field. A very similar scope of work has been of interest for control engineers in the last years, where the goal was that a flexible system should follow a certain displacement field.

* Corresponding author.
E-mail addresses: juergen.schoeftner@jku.at (J. Schoeftner), hans.irschik@jku.at (H. Irschik).

http://dx.doi.org/10.1016/j.jsv.2016.07.025

One particular case of displacement tracking is known under the notion shape control, where the deformation of the structure should vanish, or at least the motion should be manipulated in such manner that the displacements or the vibrations at specific locations are zero. An extensive literature review on this topic is presented by Irschik [9]. Shape control belongs to the class of feed-forward control methods and is an inversely posed problem: one asks for piezoelectric control eigenstrains, so that the system behaves in a desired way. When regarding the converse piezoelectric effect as a possible source for eigenstrain, this means the determination of the voltages in the piezoelectric transducers. The notions eigenstrain or eigenstress are neologisms that were first introduced by Mura [10]. Eigenstrain denotes non-elastic strains such as initial strains and plastic strains, but also expansions due to the thermal or the piezoelectric effect.

As already mentioned, shape control or tracking problems are inversely posed mathematical problems, where even linear systems might have no solution, one solution or several solutions. A simple example without solution is a clamped–clamped beam with a constant distribution of the piezoelectric layer: vibrations of this beam will not occur, if an electric voltage is applied across the electrodes, see Hubbard and Burke [11]. Depending on the kinematical boundary conditions and the number of redundancies, infinitely many constant or linear layer distributions may exist for statically indeterminate beams, which do not influence the motion of the structure. These distributions are also called nil-potent shape functions, see Irschik et al. [12,13]. The notion shape control was introduced by Hafka and Adelman [14] by imposing a certain temperature field working as an actuation mechanism to avoid deformations caused by external disturbances. For slender piezoelectric beams, force induced vibrations are annihilated, if the quasi-static bending moment of the smart control devices is equal, but sign-reversed to the quasi-static moment caused by the external forces, see Irschik et al. [13]. This result was experimentally verified by Nader [15]. Irschik and Pichler et al. [16] showed that the distribution of the actuating stress has to be equal to the statically admissible stress in order to avoid vibrations of linear elastic structures. An innovative static and dynamic shape control method of a cantilever beam was performed in Schoeftner et al. [17]. The displacements and/or structural oscillations at several locations along the beam were nullified by tuning the necessary patch voltage with a resistive circuit network. The experimental setup finally proved the theory. Further applications of shape control include the following: Austin et al. [18] designed and constructed adaptive wings, which included actuators to minimize the aerodynamic performance. Agrawal and Treanor [19] minimized a quadratic cost function of an unloaded cantilever, which contains the error between desired and achieved static deflection, to obtain the best locations for the piezoceramics actuators. Krommer and Varadan [20,21] studied the control of the motion of certain subdomains of thin plates by applying a suitable distribution of the piezoelectric actuation. The idea of shape control for beams was extended for passive structures in case of time-harmonic disturbances, see Schoeftner and Irschik [22,23].

To the best knowledge of the present authors, stress tracking or stress annihilation has been rarely treated in such a systematic way as displacement tracking or shape control. Mechanical stress is understood as the driving factor for the collapse, material fatigue and damage of structures, if a certain stress level is exceeded. In Irschik [24] it has been discussed how to obtain a certain stress field by prescribing the local and temporal control actuation in order to achieve a certain stress or displacement tracking field. A link between shape control and stress tracking is given in Irschik et al. [25]: by means of a three-dimensional formulation and taking into account eigenstrain actuation and an arbitrary external load, it was found that the stress distribution in a body, where the displacements are completely annihilated by eigenstrain actuation, is equal to the quasi-static stress distribution caused by the external load.

In this contribution we focus on stress tracking of a slender bar. Our paper is organized as follows: after recalling the fundamental relations, such as the equations of motion and the constitutive relations of slender bar, we derive the differential equation of the stress (=partial differential equations in terms of the axial stress) in Section 2. In Section 3 we define the error displacement and the error stress. These are the differences between the actual and the desired displacement and stress. A semi-positive definite time-dependent integral is defined, which contains the squares of the derivatives of the error stress with respect to the time and the spatial coordinate. By showing that the time-derivative of this integral is zero, one finds conditions for the control eigenstrain depending on the imposed forces and on the desired stress. Finally, in Section 4, two examples are presented which illustrate our derived control feed-forward control algorithm. First we show under which conditions the force induced stress of a clamped–free bar can be annihilated. Then we realize a desired stress distribution of a support-excited bar with an attached mass by proper control actuation of the piezoelectric transducer.

2. Stress tracking problem of a piezoelectric bar

The simplest form of the equations of motion of a bar, within the framework of the one-dimensional linear theory of elasticity, can be written as, see Ziegler [4]

$$\rho\ddot{u}(x,t) = b(x,t) + \sigma_{,x}(x,t), \tag{1}$$

where ρ is the density and σ and u are the axial stress and the axial displacement, respectively. The axial coordinate is x, and t stands for the time. The spatial and the time derivatives are denoted by $(\ldots)_{,x}$ and $\dot{(\ldots)}$, respectively. We consider only small deformations of some solid body, so we are within the framework of the linear theory of elasticity. This structure is subjected to the generally transient force loading $b(x,t)$. Considering a thermomechanical, a piezoelectric or an elastomagnetic

material, the constitutive relations read

$$\sigma(x,t) = C[\varepsilon(x,t) - \varepsilon_c(x,t)]. \tag{2}$$

The axial strain $\varepsilon = u_{,x}$ and the elastic modulus on beam level is denoted as C. The eigenstrain is denoted by ε_c, see Mura [10]. In the following, ε_c is used as a control input, in order to solve the stress tracking problem. Combining Eqs. (1) and (2) the hyperbolic partial differential equation reads

$$\rho\ddot{u}(x,t) - Cu_{,xx}(x,t) = b(x,t) - C\varepsilon_{c,x}(x,t). \tag{3}$$

Initially, at time $t=0$ the displacement and the velocity field are given by $u(x,0) = U(x)$ and $\dot{u}(x,0) = V(x)$, respectively. Taking into account the geometric (or kinematic) boundary conditions at ∂B_u and the natural (or dynamic) boundary conditions at ∂B_σ

$$\begin{aligned} \partial B_u: &\quad u(x,t) = u_0(t) \\ \partial B_\sigma: &\quad \sigma(x,t) = \sigma_0(t) \end{aligned} \tag{4}$$

an analytical or a numerical solution of Eq. (3) can be obtained as a function of time t and place x.

In order to derive the stressed-based differential equation, Eq. (2) is differentiated twice with respect to t, yielding

$$\ddot{\varepsilon}(x,t) = \ddot{u}_{,x}(x,t) = \ddot{\varepsilon}_c(x,t) + \frac{1}{C}\ddot{\sigma}(x,t). \tag{5}$$

Differentiating the equations of motion (1) with respect to x and using Eq. (5), the partial differential equations for the stress read

$$C\sigma_{,xx}(x,t) = \rho[\ddot{\sigma}(x,t) + C\ddot{\varepsilon}_c(x,t)] - Cb_{,x}(x,t). \tag{6}$$

We see that the reformulation of the governing equations of motion yields a hyperbolic partial differential equation for $\sigma(x,t)$. In order to derive a solution, initial conditions and boundary conditions have to be prescribed.

3. Problem statement, error dynamics and stress tracking conditions

The goal of the present paper is to derive conditions in order to manipulate the stress field $\sigma(x,t)$. It has been already discussed above that piezoelectric control devices are popular candidates to control the deformation of a flexible system. Here, we ask if it is possible to prescribe a desired stress field within the bar. The corresponding problem is called stress-tracking problem.

We introduce the error stress σ_e as

$$\sigma_e = \sigma_f + \sigma_c - \sigma_d, \tag{7}$$

where the desired stress is denoted by σ_d. The variables σ_f and σ_c are the additive decomposition of the stress due to the imposed force and the control eigenstrain, respectively. In a similar manner the error displacement u_e is split up into the actual displacement (=the disturbance u_f and the control force u_c) and the desired displacement u_d

$$u_e = u_f + u_c - u_d. \tag{8}$$

For the derivation of conditions for stress tracking we define the following integral over the length of the bar:

$$I_\sigma(t) = \int_x \left(\frac{1}{\rho}\sigma_{e,x}^2 + \frac{1}{C}\dot{\sigma}_e^2\right) \mathrm{d}x. \tag{9}$$

This integral is a semi-positive definite integral since it holds $\rho > 0$ and $C > 0$. It was introduced by Hetnarski and Ignaczak [1] for checking the uniqueness of the dynamic tracking boundary problem in a three-dimensional setting, using total stresses. A three-dimensional counterpart has been introduced in the present context in Irschik et al. [25]. Here we are interested in a vanishing error stress at every time instant $\sigma_e(x,t) = 0$: if we can show that $I_\sigma(t) = 0$ holds, it follows that the error stress and its time-derivative also have to vanish. We will demonstrate this by the following two steps:

- First step: we show that the integral (9) is time-independent $\dot{I}_\sigma(t) = 0 \rightarrow I_\sigma(t) = I_\sigma(0)$.
- Second step: we intend to nullify the error stress $\sigma_e(t)$ at every time-instant t and at every location x. Consequently, the spatial and temporal derivatives at $t=0$ read $\sigma_{e,x}(x,0) = \dot{\sigma}_e(x,0) = 0$, causing that according to Eq. (9) $I_\sigma(0) = 0$ holds.

3.1. First step (show that $\dot{I}_\sigma(t) = 0$)

In the first step we differentiate Eq. (9) with respect to time, finding that

$$\frac{\dot{I}_\sigma(t)}{2} = \int_x \left(\frac{1}{\rho}\sigma_{e,x}\dot{\sigma}_{e,x} + \frac{1}{C}\dot{\sigma}_e\ddot{\sigma}_e\right) \mathrm{d}x. \tag{10}$$

Applying integration by parts to the first term on the right-hand side, one can alternatively write

$$\frac{1}{\rho}\sigma_{e,x}\dot{\sigma}_{e,x}=\frac{1}{\rho}\left[-\sigma_{e,xx}\dot{\sigma}_e+\left(\sigma_{e,x}\dot{\sigma}_e\right)_{,x}\right]. \tag{11}$$

Inserting Eqs. (6), (7) and (11) into (10) one finds

$$\frac{\dot{I}_\sigma(t)}{2}=\int_x\left[\frac{1}{\rho}\left(b+\sigma_{d,x}\right)_{,x}-\frac{1}{C}\ddot{\sigma}_d-\ddot{\varepsilon}_c\right]\dot{\sigma}_e\mathrm{d}x+\int_x\frac{1}{\rho}\left(\sigma_{e,x}\dot{\sigma}_e\right)_{,x}\mathrm{d}x. \tag{12}$$

Note that the integral containing $\ddot{\sigma}_e$ in Eq. (10) has canceled out. The second term on the right-hand side in Eq. (12) follows to

$$\int_x\frac{1}{\rho}\left(\sigma_{e,x}\dot{\sigma}_e\right)_{,x}\mathrm{d}x=\frac{1}{\rho}\left[\sigma_{e,x}\underbrace{\left(\dot{\sigma}_f+\dot{\sigma}_c-\dot{\sigma}_d\right)}_{=\dot{\sigma}_e\ \text{see Eq.(7)}}\right]\Bigg|_{\partial B_\sigma}+\dot{\sigma}_e\underbrace{\left[-\frac{1}{\rho}\left(b+\sigma_{d,x}\right)+\left(\ddot{u}_f+\ddot{u}_c\right)\right]}_{=\sigma_{e,x}/\rho\ \text{see Eqs.(1), (7), (8)}}\Bigg|_{\partial B_u}. \tag{13}$$

Finally the time-derivative of the positive definite integral equation (12) becomes

$$\frac{\dot{I}_\sigma(t)}{2}=\int_x\left[\frac{1}{\rho}\left(b+\sigma_{d,x}\right)_{,x}-\frac{1}{C}\ddot{\sigma}_d-\ddot{\varepsilon}_c\right]\dot{\sigma}_e\mathrm{d}x+\frac{1}{\rho}\left[\sigma_{e,x}\left(\dot{\sigma}_f+\dot{\sigma}_c-\dot{\sigma}_d\right)\right]\Big|_{\partial B_\sigma}+\dot{\sigma}_e\left[-\frac{1}{\rho}\left(b+\sigma_{d,x}\right)+\left(\ddot{u}_f+\ddot{u}_c\right)\right]\Bigg|_{\partial B_u}. \tag{14}$$

As it can be seen from (14), the integral (9) is constant in time, if the following conditions are guaranteed by the control input $\ddot{\varepsilon}_c$:

$$\ddot{\varepsilon}_c=\frac{1}{\rho}\left(b+\sigma_{d,x}\right)_{,x}-\frac{1}{C}\ddot{\sigma}_d, \tag{15}$$

and if the following relations hold at the geometric (kinematic) and/or natural (dynamic) boundaries

$$\partial B_\sigma:\quad \dot{\sigma}_c=-\dot{\sigma}_f+\dot{\sigma}_d \tag{16}$$

$$\partial B_u:\quad \ddot{u}_c=-\ddot{u}_f+\frac{1}{\rho}\left(b+\sigma_{d,x}\right). \tag{17}$$

The final solution of the control eigenstrain ε_c in Eq. (15) is obtained by integrating twice with respect to time, from which follows that

$$\varepsilon_c=\iint\left[\frac{1}{\rho}\left(b+\sigma_{d,x}\right)_{,x}\right]\mathrm{d}t\mathrm{d}t-\frac{1}{C}\sigma_d+K_1(x)t+K_0(x). \tag{18}$$

The determination of the integration functions $K_0(x), K_1(x)$ is also treated in Section 3.2.

3.2. Second step (show that $I_\sigma(0)=0$)

Substituting Eqs. (2) and (7) into Eq. (9), one finds that

$$\begin{aligned}I_\sigma(0)=&\int_x\frac{1}{\rho}\left[Cu_{f,xx}(x,t)+Cu_{c,xx}(x,t)-C\varepsilon_{c,x}(x,t)-\sigma_{d,x}(x,t)\right]^2\mathrm{d}x|_{t=0}\\&+\int_x\frac{1}{C}\left[C\dot{u}_{f,x}(x,t)+C\dot{u}_{c,x}(x,t)-C\dot{\varepsilon}_c(x,t)-\dot{\sigma}_d(x,t)\right]^2\mathrm{d}x|_{t=0}.\end{aligned} \tag{19}$$

If the control initial data is chosen such that

$$\begin{aligned}t=0:\quad Cu_{c,x}(x,0)-C\varepsilon_c(x,0)&=-Cu_{f,x}(x,0)+\sigma_d(x,0)\\C\dot{u}_{c,x}(x,0)-C\dot{\varepsilon}_c(x,0)&=-C\dot{u}_{f,x}(x,0)+\dot{\sigma}_d(x,0),\end{aligned} \tag{20}$$

then one observes that $I_\sigma(0)=0$ in Eq. (19) and, consequently, the error stress $\sigma_e(x,t)$ is zero at every time instant t and every location x. By prescribing the initial conditions of the problem (i.e. $u(x,0)=U(x)=u_c(x,0)+u_f(x,0)$ and $\dot{u}(x,0)=V(x)=\dot{u}_c(x,0)+\dot{u}_f(x,0)$) and the desired initial stress distribution (i.e. $\sigma_d(x,0)$ and $\dot{\sigma}_d(x,0)$), the initial values of the control input data $\varepsilon_c(x,0), \dot{\varepsilon}_c(x,0)$ are known from Eq. (20), and so also the x-dependent functions $K_0(x), K_1(x)$ can be determined from Eq. (18).

4. Examples – controlling the axial stress of a bar

In this section we verify our stress-control conditions (15)–(17) by studying two examples. A piezoelectric bar is considered, where we assume that the transverse piezoelectric constant e_{31} is responsible for the axial eigenstrain, it holds $\varepsilon_c(x,t)=e_{31}E_z(x,t)/C$. The electric field in the z-direction is given by the ratio of the electric voltage $V(x,t)$ and the thickness

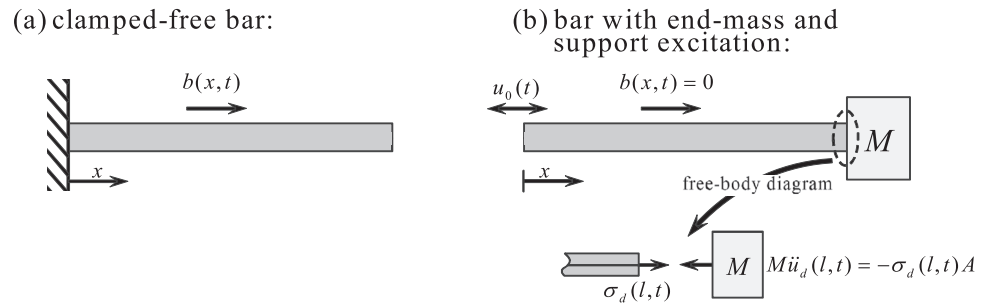

Fig. 1. (a) A piezoelectric clamped–free bar which is force-excited by $b(x,t)$. (b) A piezoelectric support-excited bar with $u(0,t)=u_0(t)=B(\alpha t)^3 e^{-\alpha t}$.

Table 1
Parameters for the numerical examples.

Variable (unit)	Value	Description
ρ(kg m^{-3})	7750	Density
h (m)	$8.00\cdot 10^{-4}$	Thickness
b (m)	$5.00\cdot 10^{-2}$	Width
e_{31} (A s m^{-2})	-10.94	Piezoelectric modulus
C (N m^{-2})	$6.29\cdot 10^{10}$	Young's modulus
M(kg)	10	End mass
l (m)	0.8	Length

h in the following manner: $E_z(x,t)=V(x,t)/h$, see also Buchberger and Schoeftner [26] for a realization of the x-dependency of the applied voltage by using so-called moderately conductive electrodes.

First, a clamped–free bar (Fig. 1a) is treated in Section 4.1, where the mechanical stress due to the force load is required to vanish. At the end of the chapter numerical results are shown if the stress control condition at the clamped end is not perfectly fulfilled. In Section 4.2, a bimorph bar with end mass is considered (Fig. 1b) whose motion at the left end is prescribed. Numerical results are given for three different support excitation profiles.

The geometrical and material parameters for the piezoelectric two-layer bar are given in Table 1. For the simulation, the wave equation (3) of the bar is discretized in 50 finite elements (FE). As interpolation functions for the displacement of the elements, linear ansatz functions are used, see e.g. Bathe [27]. For the stress-controlled case, the accuracy of our numerical approach can be easily tested by comparing the analytical displacement and the stress at several locations (for example 1 (Section 4.1) see Eqs. (28) and (27) and for example 2 (Section 4.2) see Eqs. (33) and (35)).

4.1. Example 1: clamped–free piezoelectric bar (Fig. 1a)

For this configuration our goal is that the desired stress should vanish at every point and at any time: $\sigma_d(x,t)=0$. The distributed external force is considered in the form

$$b(x,t)=-K\left[1-x/l-\beta\left(1-\frac{x^2}{l^2}\right)\right]\omega^2\cos(\omega t), \tag{21}$$

where β is considered as an arbitrary parameter.

4.1.1. Conditions for zero-stress $\sigma_d(x,t)=0$

Two conditions at the boundaries, see Eqs. (16) and (17), need to be satisfied for stress control. Since no single external force acts at the right end $x=l$, see Eq. (16), it holds

$$\dot{\sigma}_c(l,t)=-\dot{\sigma}_f(l,t)=0 \tag{22}$$

At the clamped end $x=0$, Eq. (17) is only true if the condition $\beta=1$ holds:

$$\frac{1}{\rho}b(0,t)=-\frac{K}{\rho}(1-\beta)\omega^2\cos(\omega t)=0 \quad \text{for} \quad \beta=1. \tag{23}$$

For $\beta\neq 1$ the external force does not vanish $b(0,t)\neq 0$, i.e. the stress level does not vanish at the clamped end. Taking into account the initial conditions

$$u(x,0)=\dot{u}(x,0)=0, \tag{24}$$

the necessary control eigenstrain is obtained from Eqs. (18) and (20) as

$$\varepsilon_c(x,t)=\frac{K}{\rho l}(2\beta x/l-1)(\cos(\omega t)-1). \tag{25}$$

4.1.2. Proof for zero-stress $\sigma_d(x,t)=0$ if $\beta=1$

Inserting the force load $b(x,t)$ and the control eigenstrain $\varepsilon_c(x,t)$ from Eq. (25) into the equations of motion (3), one finds

$$\beta=1:\quad \rho\ddot{u}(x,t)-Cu_{,xx}(x,t)=K\left[x/l-x^2/l^2\right]\omega^2\cos(\omega t)-\frac{2CK}{\rho l^2}(\cos(\omega t)-1). \tag{26}$$

The solution for this problem can be derived by means of Green's functions, see Graff [28, p. 25]. For $\beta=1$ and the initial conditions equation (24), we obtain

$$\beta=1:\quad u_(x,t)=-\frac{K}{\rho}\left(x/l-x^2/l^2\right)(\cos(\omega t)-1). \tag{27}$$

The actual stress follows from the constitutive relations (2) by taking into account Eqs. (25) and (27)

$$\beta=1:\quad \sigma(x,t)=C\left[u_{,x}(x,t)-\varepsilon_c(x,t)\right]=0, \tag{28}$$

which verifies our goal to nullify the stress distribution. The case $\beta\neq 1$ does not yield a stress-free solution, in contrast to (28). This reveals a major limitation of our stress suppression method: by means of eigenstrain actuation it is not possible to achieve an arbitrary stress level at kinematic boundaries. In our case, a vanishing stress at the kinematic boundary is only possible for $\beta=1$, which means that the imposed force $b(x,t)$ vanishes at $x=0$, see Eqs. (21) and (23).

4.1.3. Numerical results for $\beta=1$, $\beta=0.95$ and $\beta=0.9$

The variable $K=1\ \mathrm{kg\,s^{-2}}$, all other parameters can be found in Table 1. The excitation frequency is $f=100$ Hz and the first eigenfrequency of the system reads $f_1=887.5$ Hz. Fig. 2 shows the axial stress at $x=\{l/20,l/2,4l/5\}$, if the variable β is 1 (Fig. 2a and d), 0.95 (Fig. 2b and e) and 0.9 (Fig. 2c and f). Fig. 2a, b and c is denoted as controlled configurations, because the eigenstrain condition equation (25) is applied. In Fig. 2d, e and f, the eigenstrain is absent ($\varepsilon_c=0$, uncontrolled cases).

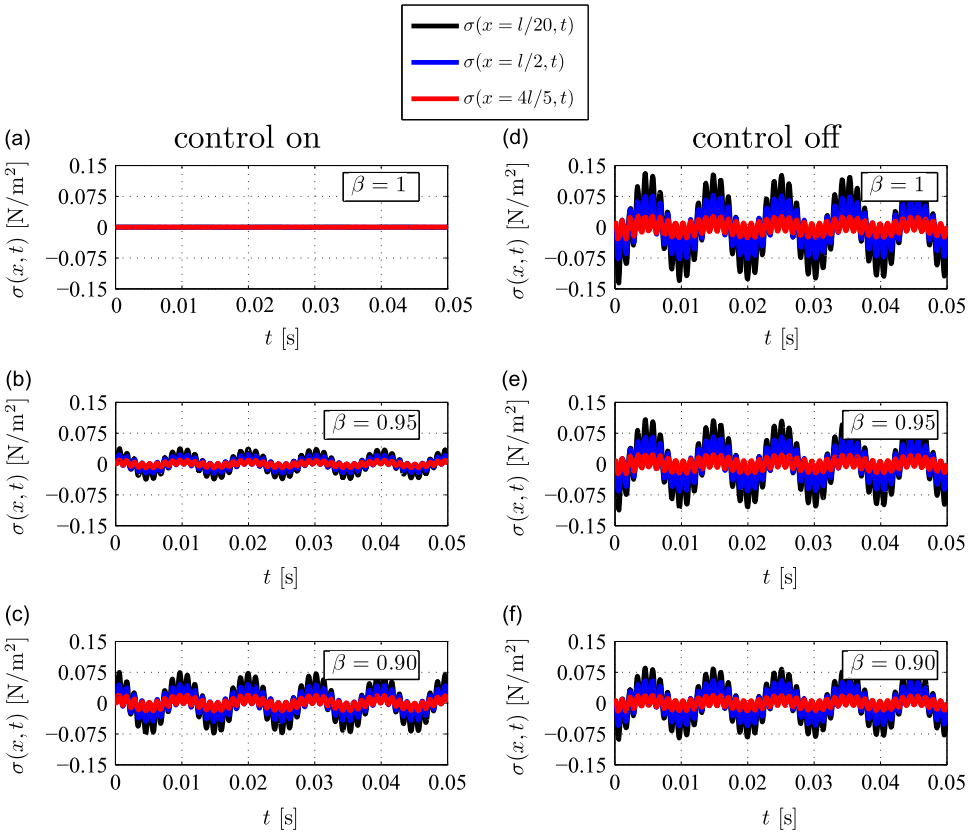

Fig. 2. Stress distribution at three locations ($x=\{l/20,l/2,4l/5\}$) for the clamped–free bar with control (ε_c chosen according to Eq. (25) for $\beta=\{1,0.95,0.9\}$, a, b, c) and without control action ($\varepsilon_c=0$ for $\beta=\{1,0.95,0.9\}$, d, e, f).

The condition in Eq. (22) for the free end is satisfied in all cases. As stated in the previous section, one observes that only for $\beta = 1$ (Fig. 2a) the stress becomes zero at all locations and at every time instant in the controlled case, because Eq. (23) is also fulfilled. For $\beta = 0.95$ and $\beta = 0.9$, the eigenstrain condition in Eq. (25) is applied, but the condition at the clamped end, Eq. (23), is now violated. For $\beta = 0.95$, the stress level turns out to be also considerably reduced in comparison to the uncontrolled bar, see Fig. 2b and e. For $\beta = 0.9$ (Fig. 2c and f), however, the results for the controlled and the uncontrolled bar are almost indistinguishable. The example shows clearly the necessity of satisfying the conditions given in Eqs. (22), (23) and (25) simultaneously in order that a complete stress suppression becomes possible. One observes that if β is close to 1 (e.g. $0.95 < \beta < 1.05$), our stress control strategy still works quite well and yields suboptimal solutions. The question, if approximate solutions of Eq. (25) (i.e. if a spatial discretization is necessary due to practical reasons) as well as solutions, in which only Eq. (22) or (23) are not met, yield similar results, is left to a future investigation.

4.2. Example 2: piezoelectric bar with prescribed boundary motion (Fig. 1b)

Next, we consider the case of a straight, homogeneous elastic bar with an end mass at the right end M. The left end is kinematically excited by

$$u(0,t) = u_0(t) = B(\alpha t)^3 \mathrm{e}^{-\alpha t} \quad \text{with } B = \frac{\mathrm{e}^3}{27} \times 0.0005. \tag{29}$$

From the kinematic boundary condition (17) one finds

$$\underbrace{\ddot{u}_f(0,t) + \ddot{u}_c(0,t)}_{\ddot{u}(0,t) = \ddot{u}_d(0,t)} = \frac{1}{\rho}\sigma_{d,x}(0,t). \tag{30}$$

From the free-body diagram (see Fig. 1b), one finds from Newton's law for the end-mass

$$M\ddot{u}_d(l,t) = -\sigma_d(l,t)A. \tag{31}$$

Taking into consideration the equations of motion of the bar $\rho\ddot{u}_d(l,t) = \sigma_{d,x}(l,t)$ at $x = l$, which relates the desired stress to the desired acceleration, one finds from Eq. (31) a condition between the desired stress and its derivative with respect to x

$$\frac{M}{\rho A}\sigma_{d,x}(l,t) = -\sigma_d(l,t). \tag{32}$$

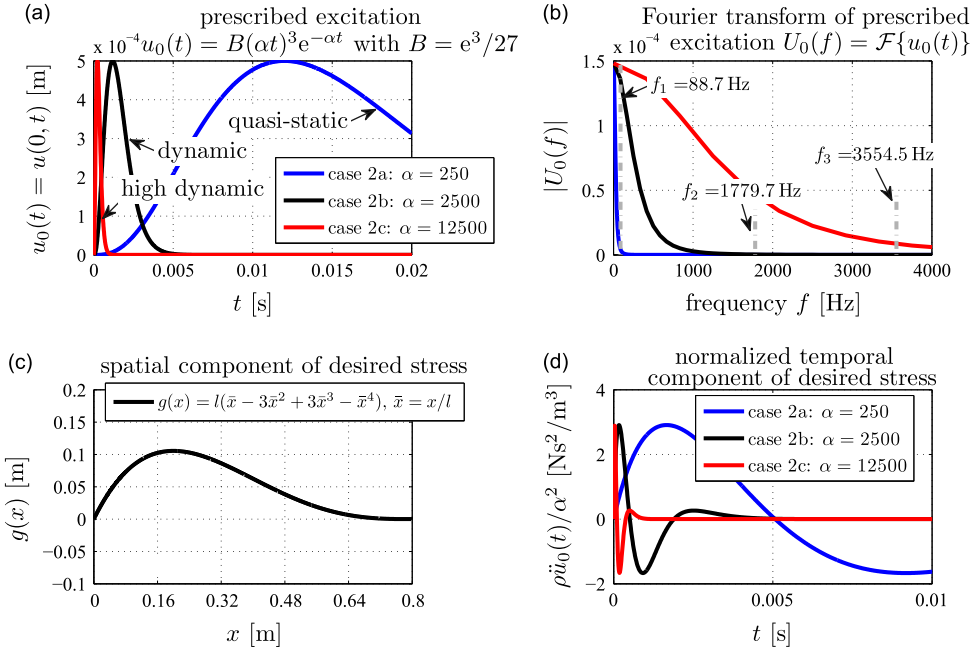

Fig. 3. (a) Transient support-excitation profile and (b) its Fourier transform, see Eq. (29), for various values of α. (c) and (d) The desired stress is separable in space and time $\sigma_d(x,t) = g(x)\rho\ddot{u}_0(t)$. The acceleration $\ddot{u}_0(t)$ is given by Eq. (29). (For interpretation of the references to color in this figure caption, the reader is referred to the web version of this paper.).

The two conditions (30) and (32) are satisfied if the desired stress is chosen as (see also Fig. 3c and d)

$$\sigma_d(x,t) = l\left(\frac{x}{l} - 3\frac{x^2}{l^2} + 3\frac{x^3}{l^3} - \frac{x^4}{l^4}\right)\rho\ddot{u}_0(t). \tag{33}$$

4.2.1. Conditions and proof for stress-tracking

Assuming trivial initial conditions $u(x,0) = \dot{u}(x,0) = 0$, the necessary eigenstrain is evaluated from Eqs. (18) and (20), yielding

$$\varepsilon_c(x,t) = \left(-\frac{6}{l} + 18\frac{x}{l^2} - 12\frac{x^2}{l^3}\right)u_0(t) - l\left(\frac{x}{l} - 3\frac{x^2}{l^2} + 3\frac{x^3}{l^3} - \frac{x^4}{l^4}\right)\frac{\rho}{C}\ddot{u}_0(t). \tag{34}$$

The analytical solution for the displacement can be derived in a similar manner as for the first example (see Section 4.1, i.e. by inserting (34) into the equations of motion (3)). It reads

$$u(x,t) = \left(1 - 6\frac{x}{l} + 9\frac{x^2}{l^2} - 4\frac{x^3}{l^3}\right)u_0(t). \tag{35}$$

Substituting (34) and (35) into the constitutive relation (2), one finds that the actual stress is equal to the desired stress given by Eq. (33).

4.2.2. Numerical simulation of the controlled and uncontrolled case

The support excitation (29) and its Fourier transform are shown in Fig. 3a and b. Simulations are performed for three different values of the parameter α:

- for the quasi-static case (blue, $\alpha = 250\ \mathrm{s}^{-1}$),
- for the dynamic case (black, $\alpha = 2500\ \mathrm{s}^{-1}$), and
- for the highly dynamic excitation (red, $\alpha = 12,500\ \mathrm{s}^{-1}$).

The eigenfrequencies of our system are $f_1 = 88.7$ Hz, $f_2 = 1779.7$ Hz and $f_3 = 3554.5$ Hz. The Fourier transform of the excitation is shown in Fig. 3b (gray dash-dot lines). This also demonstrates that the low-frequency excitation, which is called the quasi-static excitation, (blue curve) does not really excite the higher modes. In contrast, the highly dynamic excitation (red) also excites most of the higher eigenmodes, so it is expected that wave propagation phenomena will be observed for this case.

The stress distribution $\sigma(x,t)$ and the displacement $u(x,t)$ at $x = l/20 = 0.04$ m (close to the support excitation), at $x = l/2 = 0.4$ m (middle of the bar) and at $x = 4\,l/5 = 0.64$ m (close to attached mass) are shown in Figs. 4–6. Furthermore,

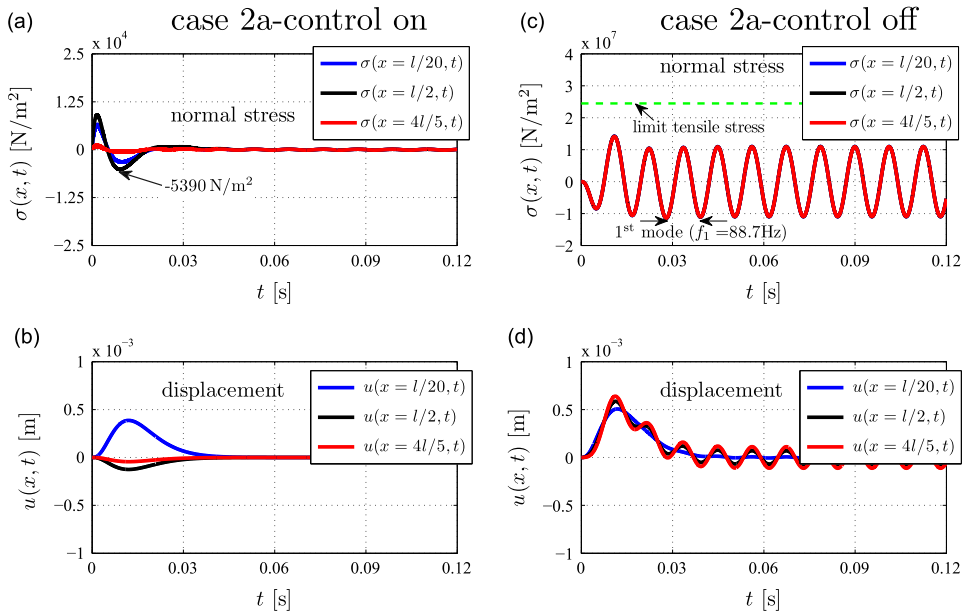

Fig. 4. Quasi-static excitation $\alpha = 250$: (a) and (c) stress distribution and (b) and (d) displacement at three locations ($x = \{l/20, l/2, 4l/5\}$) for the support-excited bar with control (ε_c chosen according to Eq. (34)) and without control ($\varepsilon_c = 0$).

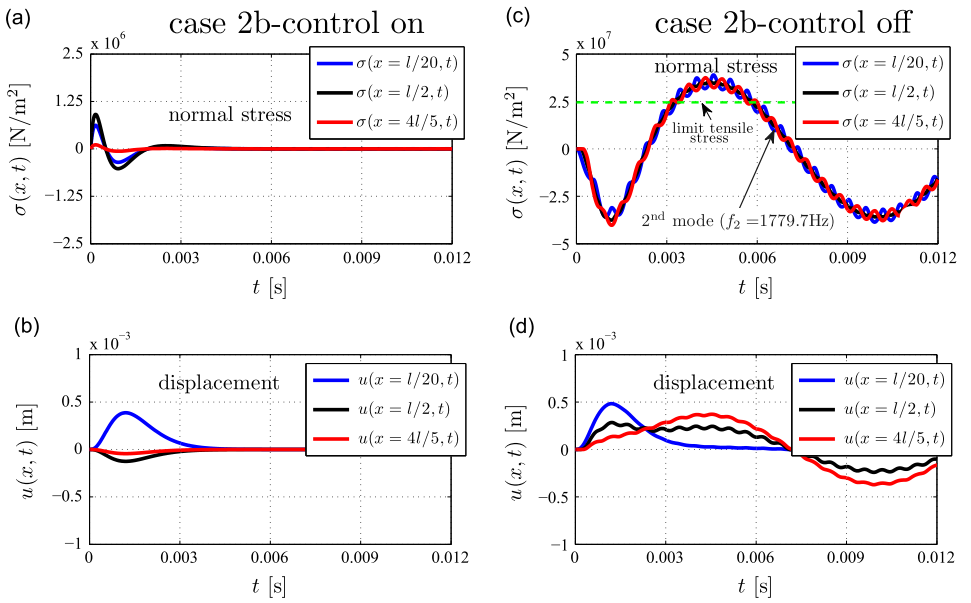

Fig. 5. Dynamic excitation $\alpha = 2500$: (a) and (c) stress distribution and (b) and (d) displacement at three locations ($x = \{l/20, l/2, 4l/5\}$) for the support-excited bar with control (ε_c chosen according to Eq. (34)) and without control ($\varepsilon_c = 0$). (For interpretation of the references to color in this figure caption, the reader is referred to the web version of this paper.)

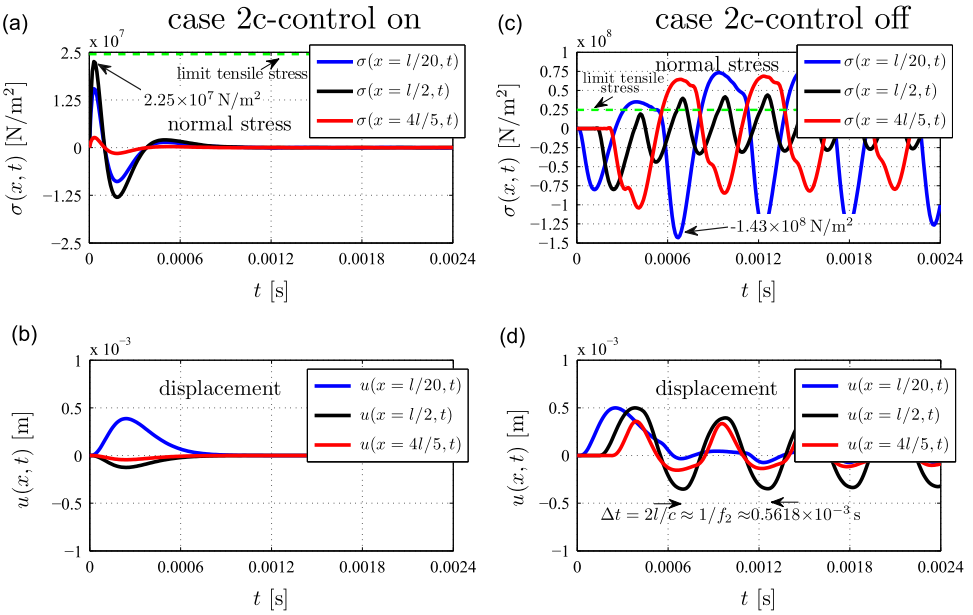

Fig. 6. High-frequency excitation $\alpha = 12,500$: (a) and (c) stress distribution and (b) and (d) displacement at three locations ($x = \{l/20, l/2, 4l/5\}$) for the support-excited bar with control (ε_c chosen according to Eq. (34)) and without control ($\varepsilon_c = 0$).

the tensile stress for non-preloaded PZT ceramics is provided by the manufacturer PI and reads 2.5×10^7 N/m^2, see [29]. This is approximately 10% of the maximum compressive pressure limit.

4.2.3. Quasi-static excitation $\alpha = 250\ \mathrm{s}^{-1}$ (case 2a)

Fig. 4 shows the result when the support excitation hardly induces any high-frequency dynamics (see Eq. (29) with $\alpha = 250\ \mathrm{s}^{-1}$). The curves on the left (Fig. 4a and b) show the stress and the displacement when our control method is activated (control on: $\varepsilon_c(x,t)$ according to (34)), those on the right (Fig. 4c and d) the results when control is deactivated (control off: $\varepsilon_c(x,t) = 0$). Fig. 4a shows the stress profile as desired in Eq. (33). It is noted that our numerical FE solution only slightly deviates from the analytical solution (e.g. at $t = 0.00932$ s one finds $\sigma_{\mathrm{ana}}(l/2,t) = -5418$ N/m^2 and $\sigma_{\mathrm{num}}(l/2,t) = -5390$ N/m^2, so the numerical solution can be considered as a reliable solution which is very close to the

exact ones, see Eq. (33) for the stress and Eq. (35) for the displacement). The order of magnitude of the stress levels of the controlled and the uncontrolled configurations is 1:1000, i.e. our desired stress tracking profile means approximately zero stress compared to the uncontrolled bar.

For the displacement (Fig. 4b and d) one observes that the deflections at the middle and at the attached mass for the stress-controlled bar are opposite in sign to the displacement of the uncontrolled case, i.e. the elastic strain is much higher for the stress-controlled bar although the stress is comparatively low. For the uncontrolled case one observes undamped superimposed vibrations with an amplitude of about 0.1 mm relative to the prescribed support deflection.

4.2.4. *Dynamic excitation* $\alpha = 2500\ \mathrm{s}^{-1}$ *(case 2b)*

Fig. 5 shows the result for $\alpha = 2500\ \mathrm{s}^{-1}$. If the control action is turned off, one observes that the first and the second eigenmode of the system are excited, see Fig. 5b and d. The stress amplitude is $3.75 \times 10^7\ \mathrm{N/m^2}$ and exceeds the level of the maximum tensile stress (see green dashed line in Fig. 5c). This is also much higher than the stress for the controlled bar, which follows the desired stress profile equation (33). A comparison of the order of the maximal stress levels (maximum stress at $t \approx 0.2$ ms is $9.4 \times 10^5\ \mathrm{N/m^2}$) yields that the stress level between controlled and uncontrolled bar is 1:40. From a practical point of view this means that zero-stress control is performed.

4.2.5. *High-frequency excitation* $\alpha = 12,500\ \mathrm{s}^{-1}$ *(case 2c)*

Fig. 6 shows the result for $\alpha = 12,500\ \mathrm{s}^{-1}$, which is the high-frequency excitation. For the uncontrolled bar one observes the typical wave propagation phenomena: it can be observed that the time $\Delta t \approx 2l/c \approx 0.5618 \times 10^{-3}$ s goes by so that the stress impulse leaves the end of the support excitation ($x=0$), then it is partially reflected by the attached mass at $x=l$ and finally arrives again at the other end, see Graff [28] for an explanation of this phenomenon. At $t = 0.7$ ms the maximum absolute stress is $1.43 \times 10^8\ \mathrm{N/m^2}$, see Fig. 6c, but also the maximum tensile stress is higher than the stress limit $2.5 \times 10^7\ \mathrm{N/m^2}$ and thus several times higher than for the controlled case (maximum stress at $t \approx 0.04$ ms is $2.25 \times 10^7\ \mathrm{N/m^2}$, see Fig. 6a).

5. Conclusion

In this contribution analytical relations are derived to control the longitudinal stress of thin elastic bars. This task is denoted as stress-tracking. Based on a one-dimensional formulation of linear elasticity and the consideration of an eigenstrain source as control agency, the partial differential equations for the axial stress are derived. Promising candidates for eigenstrains are either magnetoelastic, thermoelastic or piezoelectric effects. In the first step a semi-positive definite time-dependent integral is defined, with the time-derivation and the gradient of the error stress as input variable. The error stress is the difference between the actual stress and the desired stress. Taking into account the partial differential equation for the stress, the constitutive relation and the applied external force load, it is found that three conditions need to be fulfilled in order to achieve a desired stress distribution, or to annihilate the error stress at every time instant and at every location. Our theory is verified by two examples, analytically as well as numerically: a clamped–free bar and a support-excited bar with end mass are considered and it is shown that the stress tracking theory yields excellent results for the problems under consideration.

Acknowledgement

J. Schoeftner acknowledges support from the Austrian Science Fund FWF via the project P 26762-N30.

References

[1] R.B. Hetnarski, J. Ignaczak, *Mathematical Theory of Elasticity*, Taylor& Francis, London, 2004.
[2] E.E. Gurtin, in: S. Fluegge (Ed.), The Linear Theory of Elasticity, Encyclopedia of Physics, VIa/2, Springer-Verlag, Berlin, 1972, pp. 297–346.
[3] A.I. Lurie, Theory of Elasticity, English translation by A.K. Belyaev, Springer-Verlag, Berlin, 2005.
[4] F. Ziegler, *Mechanics of Solids and Fluids*, 2nd ed. Springer-Verlag, New York, 1998.
[5] S.O.R. Moheimani, A.J. Fleming, *Piezoelectric Transducers for Vibration Control and Damping*, Springer-Verlag, London, 2006.
[6] E.F. Crawley, Intelligent structures for aerospace: *a technology overview and assessment*, *AIAA Journal* 32 (1994) 1689–1699.
[7] D.K. Miu, *Mechatronics: Electromechanics and Contromechanics*, Springer, New York, 1993.
[8] H.S. Tzou, Multifield transducers, devices, mechatronic systems and structronic systems with smart materials, *The Shock and Vibration Digest* 30 (1998) 282–294.
[9] H. Irschik, A review on static and dynamic shape control of structures by piezoelectric actuation, *Engineering Structures* 24 (2002) 5–11.
[10] T. Mura, *Micromechanics of Defects in Solids*, 2nd ed. Martinus Nijhoff, Dordrecht, 1991.
[11] J.E. Hubbard, S.E. Burke, Distributed transducer design for intelligent structural components, in: H.S. Tzou, G.L. Anderson (Eds.), *Intelligent Structural Systems*, Kluwer Academic Publishers, Norwell, 1992.
[12] H. Irschik, M. Krommer, A.K. Belayaev, K. Schlacher, Shaping of piezoelectric sensors/actuators for vibrations of slender beams: *coupled theory and inappropriate shape functions*, *Journal of Intelligent Material Systems and Structures* 9 (1998) 546–554.
[13] H. Irschik, M. Krommer, U. Pichler, Dynamic shape control of beam-type structures by piezoelectric actuation and sensing, *International Journal of Applied Electromagnetics and Mechanics* 17 (2003) 251–258.

[14] R.T. Hafka, H.M. Adelman, An analytical investigation of shape control of large space structures by applied temperatures, *AIAA Journal* 23 (1985) 450–457.
[15] M. Nader M, Compensation of vibrations in smart structures: shape control, experimental realization and feedback control (Doctoral thesis), Johannes Kepler University Linz, Trauner, Linz, Austria, 2007.
[16] H. Irschik, U. Pichler, An extension of Neumann's method for shape control of force-induced elastic vibrations by eigenstrains, *International Journal of Solids and Structures* 41 (2004) 871–884.
[17] J. Schoeftner, G. Buchberger, A. Brandl, H. Irschik, Theoretical prediction and experimental verification of shape control of beams with piezoelectric patches and resistive circuits, *Composite Structures* 133 (2015) 746–755.
[18] F. Austin, M.J. Rossi, W. Van Nostrand, G. Knowles, Static shape control of adaptive wings, *AIAA Journal* 32 (1994) 1895–1901.
[19] B.N. Agrawal, K.E. Treanor, Shape control of a beam using piezoelectric actuators, *Smart Materials and Structures* 8 (1999) 729–740.
[20] M. Krommer, V.V. Varadan, Control of bending vibrations within sub-domains of thin plates—Part I: *theory and exact solution*, *Journal of Applied Mechanics* 72 (2005) 432–444.
[21] M. Krommer, V.V. Varadan, 2006 Control of bending vibrations within sub-domains of thin plates—Part II: *piezoelectric actuation and approximate solution*, *Journal of Applied Mechanics* 73 (2006) 259–267.
[22] J. Schoeftner, H. Irschik, Passive damping and exact annihilation of vibrations of beams using shaped piezoelectric layers and tuned inductive networks, *Smart Materials and Structures* 18 (2009) 125008. (9 pp).
[23] J. Schoeftner, H. Irschik, Passive shape control of force-induced harmonic lateral vibrations for laminated piezoelastic Bernoulli–Euler beams—theory and practical relevance, *Smart Structures and Systems* 7 (2011) 417–432.
[24] H. Irschik, Generation of transient desired displacement or stress fields in force loaded solids and structures by smart actuation, in: Book of Abstracts of XXXV Summer School Advanced Problems in Mechanics (APM 2007), June 20–28, Repino, Saint-Petersburg, Russia, 2007.
[25] H. Irschik, M. Gusenbauer, U. Pichler, Dynamic stress compensation by smart actuation, in: R.C. Smith (Ed.), Proceedings of SPIE on Smart Structures and Materials 2004: Modeling, Signal Processing, and Control, vol. 5383, Paper no. 386, March 20–28, San Diego, CA, 2004, March 15–18, 2004.
[26] G. Buchberger, J. Schoeftner, Modeling of slender laminated piezoelastic beams with resistive electrodes—comparison of analytical results with three-dimensional finite element calculations, *Smart Materials and Structures* 22 (2013) 032001. (13pp).
[27] K.J. Bathe, *Finite Element Procedures*, Prentice Hall, 1996.
[28] K.F. Graff, *Wave Motion in Elastic Solids*, Dover, New York, 1991.
[29] Website of a Manufacturer for Piezocreamic Patches, ⟨http://www.piezo.ws/piezoelectric_actuator_tutorial/Piezo_Design_part3.php⟩, June 6, 2016.